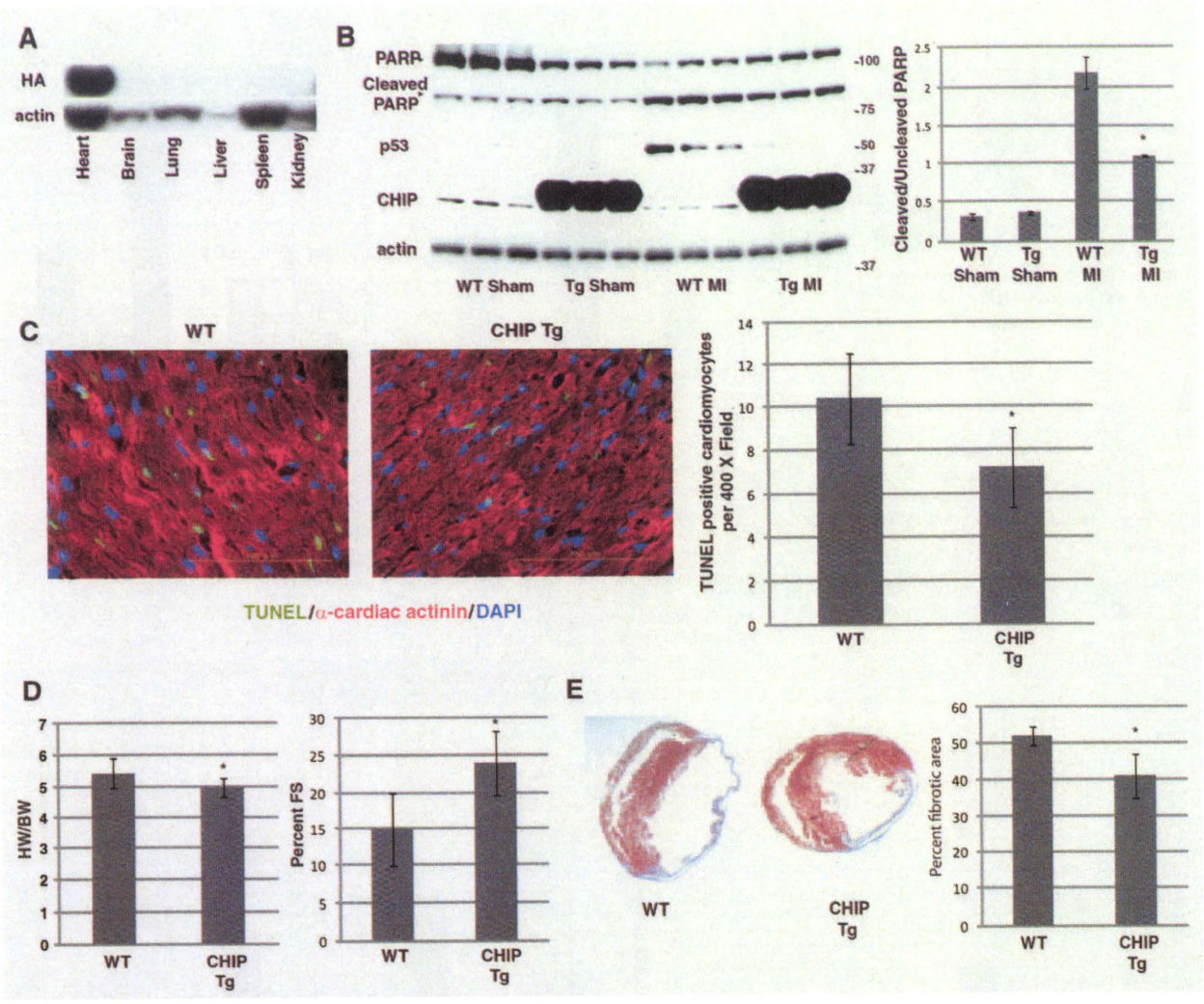

Figure 5. Overexpression of CHIP attenuates ischemic cardiac injury in vivo. A, Cardiac-specific expression of HA-tagged human CHIP in CHIP-Tg mice. **B and C,** p53 accumulation **(B)** and apoptosis 1 day after MI are reduced in CHIP-Tg mice. Apoptosis was assessed by cleaved PARP expression **(B)** and TUNEL staining **(C)**. Cleaved PARP level was assessed by densitometric analysis on band intensity of cleaved PARP over uncleaved PARP. $P<0.05$ vs WT; n=3. WT indicates wild-type mice. **D and E,** Postinfarct cardiac remodeling is attenuated in CHIP-Tg mice (n=15). HW/BW ratio **(D, left)**, contractile function **(D, right)**, and percentage fibrotic area **(E)**. *$P<0.01$ vs WT (n=30).

and less ventricular remodeling (Figure 6C and 6D). Interestingly, the effects of 17-AAG were greater than CHIP overexpression (compare Figures 5 and 6), suggesting that 17-AAG possesses cardioprotective activities that do not involve CHIP-mediated p53 degradation. As protein stability of cardioprotective proteins such as Hsp70 and HSF-1 was increased in vitro (Online Figure IV, B and C), we have examined the expression of these proteins in 17-AAG–treated mice. As expected, expression of these two proteins were increased by 17-AAG treatment (Online Figure IV, D), indicating that 17-AAG exerts its antiapoptotic effects by at least two mechanisms, one by inducing CHIP-mediated p53 degradation and the other by increasing cardioprotective heat shock proteins.

Finally, we examined the contribution of CHIP-mediated p53 degradation on the cardioprotective effects of 17-AAG. For that purpose we used CHIP heterozygous mice. There were no differences in cleaved PARP level (Figure 7A; compare WT Sham and Het Sham) or cardiac function between CHIP heterozygous mice and wild-type littermates at the basal level (Table). Following coronary artery ligation, however, apoptotic cell death was observed more prominently in CHIP heterozygous mice as assessed by increased cleaved PARP level (Figure 7A; compare WT MI and Het MI) and increased TUNEL positive cells (Figure 7B). The level of p53 accumulation was comparable following myocardial infarction between wild-type and CHIP heterozygous mice, suggesting the presence of p53 independent mechanisms for enhanced apoptosis caused by CHIP haploinsufficiency. Chronically, CHIP heterozygous mice showed worse cardiac function and worse ventricular remodeling compared with wild-type mice (Figure 7C and 7D). 17-AAG treatment was less effective to reduce p53 protein level, cleaved PARP level (Figure 7A; compare Het MI and Het MI 17-AAG), and TUNEL positive cardiomyocytes in CHIP heterozygous mice, possibly as a result of CHIP haploinsufficiency. 17-AAG treatment had minimal effects on improvements of cardiac function and ventricular remodeling on CHIP heterozygous mice also in the chronic phase (Figure 7C and 7D).

However, we must emphasize that the effects of 17-AAG were not fully attributable to CHIP-mediated p53 degradation

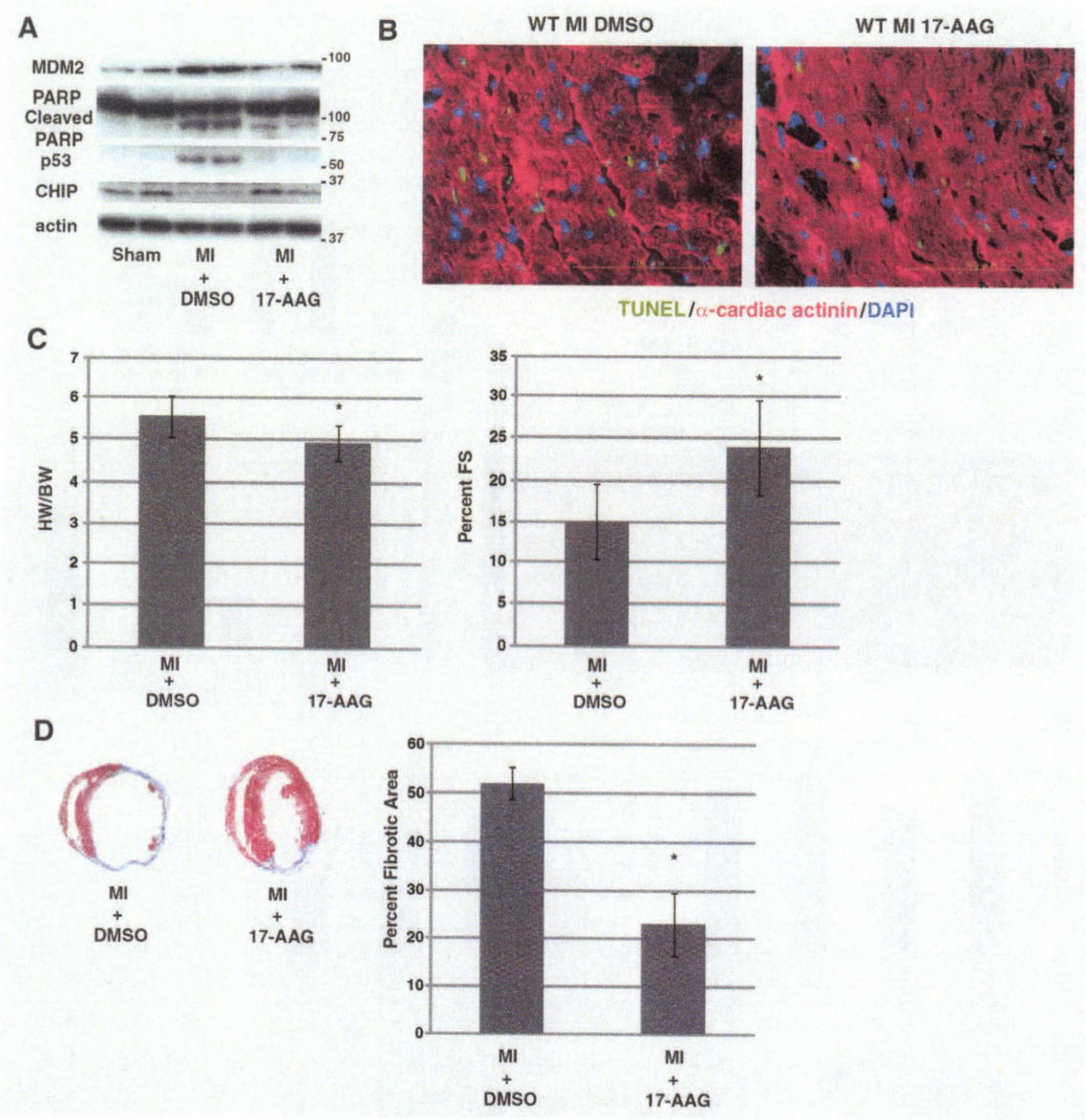

Figure 6. 17-AAG treatment attenuates ischemic cardiac injury in vivo. A, Accumulation of p53 and cleaved PARP in the heart after MI are reduced by 17-AAG treatment. 17-AAG (10 mg/kg) or vehicle was injected immediately after coronary ligation. **B,** Apoptotic cardiomyocytes at 1 day after MI was reduced in 17-AAG–treated mice. Apoptosis was assessed by TUNEL staining. **C and D,** Postinfarct cardiac remodeling is attenuated by 17-AAG treatment (n=20). HW/BW ratio **(C, left)**, contractile function **(C, right)**, and fibrotic area **(D)**. *$P<0.001$; vs MI+DMSO (n=30).

because upregulation of heat shock proteins by 17-AAG was also impaired in CHIP heterozygous mice (Figure 7A; compare WT MI 17-AAG and Het MI 17-AAG). Therefore, it would be fair to conclude that 17-AAG exerts multiple cardioprotective effects after myocardial infarction and at least one of its effects were mediated by promotion of CHIP-mediated p53 degradation.

Discussion

In the present study, we found that accumulation of p53 protein after myocardial ischemia is initiated by HIF-1 dependent downregulation of CHIP level. We have found that CHIP overexpression decreased the amount of p53 and prevented myocardial apoptosis and ameliorated ventricular remodeling after myocardial infarction. We have also found that Hsp90 inhibitor, 17-AAG, exerted similar antiapoptotic and cardioprotective effects after myocardial infarction and showed that these effects of 17-AAG was at least in part mediated by promotion of CHIP-mediated p53 degradation.

Although hypoxic stimuli have been reported to raise p53 protein levels in a variety of cell types, molecular mechanisms of p53 accumulation have been largely unknown. In the present study, we unveiled that downregulation of CHIP protein is critically involved in this process. We found that CHIP expression was downregulated after hypoxic stress through HIF-1–mediated suppression of *CHIP* promoter (Figure 2). We also found that overexpression of CHIP attenuated the p53 accumulation after hypoxic stress (Figures 4A and 5B). These results

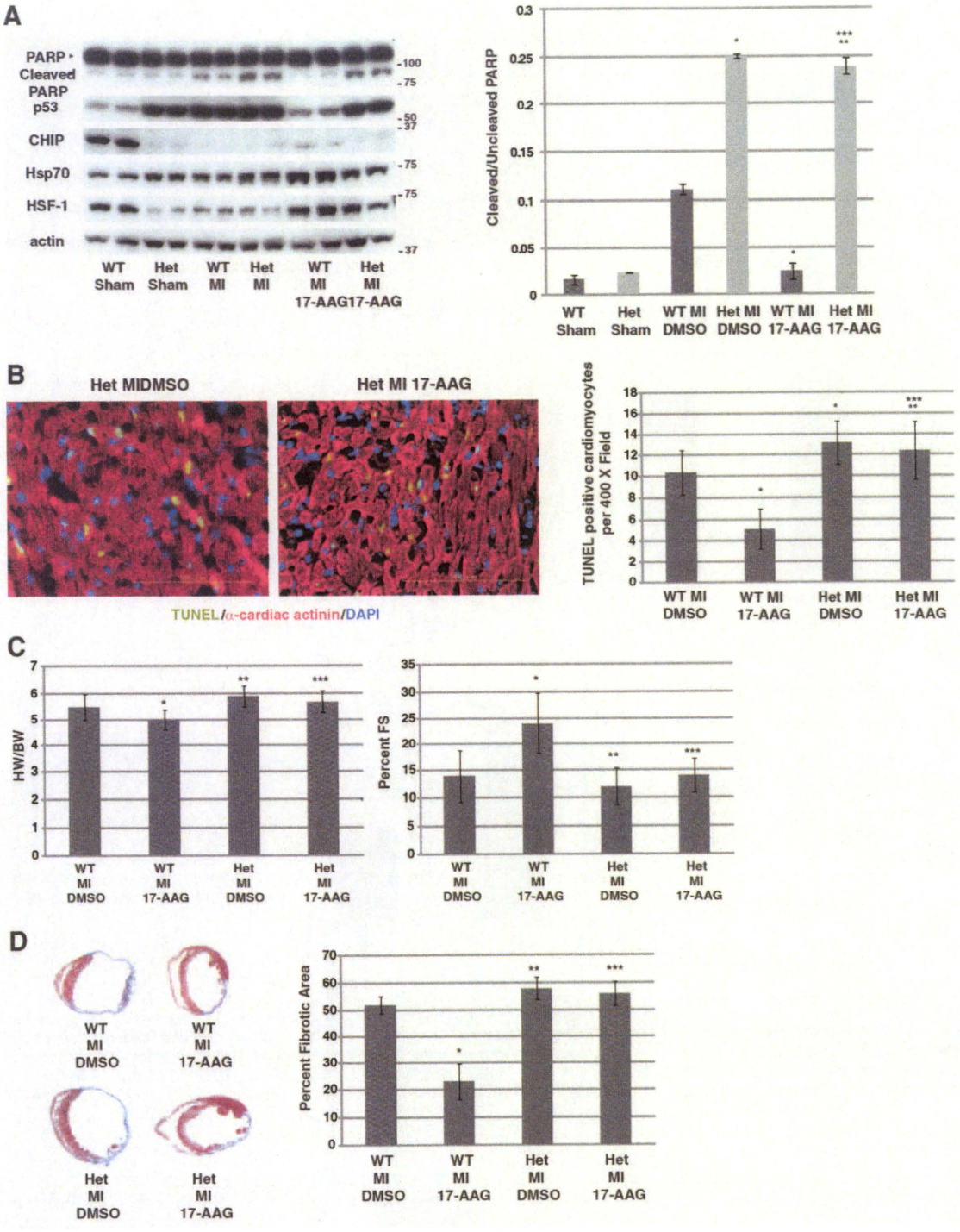

Figure 7. The effect of 17-AAG was dependent on CHIP-mediated p53 degradation and upregulation of heat shock proteins. A, 17-AAG–induced reduction of p53 accumulation and PARP expression was not observed in the heart of CHIP heterozygous mice (Het). Notably, upregulation of heat shock proteins by 17-AAG was ameliorated in CHIP heterozygous mice. **B,** Apoptotic cardiomyocytes on 1 day after MI was reduced in 17-AAG–treated mice, but this antiapoptotic effect of 17-AAG after MI was ameliorated in CHIP heterozygous mice. Apoptosis was assessed by cleaved PARP expression **(A)** and TUNEL staining **(B)**. *P<0.01 vs WT+MI+DMSO; **P<0.01 vs WT+MI +17-AAG; ***P=NS vs Het+MI+DMSO n=5. WT indicates wild-type mice; Het, CHIP heterozygous mice. **C,** 17-AAG–induced attenuation of postinfarct cardiac remodeling is less in CHIP hetero knockout mice than in wild-type mice. HW/BW ratio **(C, left)**, contractile function **(C, right)**, and fibrotic area **(D)**. *P<0.001; **P<0.05 vs WT+MI+DMSO; ***P=NS vs Het+MI+DMSO. WT+MI+DMSO: n=30; WT+MI +17-AAG: n=20; Het+MI+DMSO: n=15; Het+MI +17-AAG: n=15. WT indicates wild-type mice.

Table. Basal Characterization of the Mice Used in this Study

	Body Weight (g)	LVEDD (mm)	LVESD (mm)	IVS (mm)	LVPW (mm)	%FS
Wild type	26.3±1.2	3.12±0.12	1.04±0.02	0.72±0.02	0.74±0.02	66.7±1.3
CHIP hetero KO	25.6±0.8	3.10±0.08	1.05±0.03	0.74±0.03	0.78±0.02	66.1±0.8
CHIP Tg	26.9±1.5	3.14±0.16	1.05±0.04	0.75±0.02	0.75±0.05	66.6±1.8

suggest that hypoxic stress downregulates CHIP, leading to decreased CHIP-mediated proteolysis of p53 protein and accumulation of p53 protein. This mechanism seems to be a 'fine-tuning' of HIF-1 activity because p53 protein has been reported to bind to and inhibit HIF-1 activity.[16] After hypoxia, first HIF-1 accumulates and induces angiogenic genes, to promote angiogenesis. Thereafter, as a negative feedback loop, HIF-1 induces downregulation of *CHIP* expression and p53 accumulates, then accumulated p53 inhibits HIF-1 activity.[35] In general, this feedback system might have an antitumor effect, because in many tumor cells HIF-1 induces feeding vessels in hypoxic tumors and promotes tumor growth. HIF-1-induced, CHIP-mediated p53 accumulation acts to suppress tumor growth by (1) suppressing HIF-1 activity and blocking neovascularization and (2) inducing p53-mediated apoptosis of tumor cells. However, in the heart, this negative feedback system worsens hypoxic situation by blocking neovascularization[16] and by inducing apoptosis (this study).

The important role of apoptosis in the progression of ventricular remodeling and the possibility of antiapoptotic approach against heart failure has already been elegantly shown by Wencker et al.[3] Antiapoptotic approach after myocardial infarction has been reported to be cardioprotective not only in ischemia-reperfusion model but also in permanent coronary ligation model.[21,36,37] Therefore, inhibition of apoptotic death does not only reduce initial infarct size but also prevents ventricular remodeling through inhibiting apoptosis in the border zone of the infarct.

Accumulation of p53 has been reported to initiate many proapoptotic triggers.[38] In the heart, p53 accumulates (Figure 3C) and p53-dependent apoptosis occurs[39] after permanent coronary occlusion. We have also observed that *p53* gene deletion lead to less ventricular remodeling after myocardial infarction.[16] In the present study, we have shown that CHIP overexpression or 17-AAG treatment could prevent cardiomyocyte apoptosis and ameliorate ventricular remodeling after myocardial infarction. We have also shown some evidences that inhibition of p53 accumulation is at least one of the mechanisms for the effect of CHIP overexpression and 17-AAG. However, it should be noted that Hsp90 chaperones various proteins including prosurvival factors such as Akt/protein kinase B[40] in tumor cells and that Hsp90 inhibitors induced degradation of aberrantly overexpressed prosurvival factors in those tumor cells. Although the nature of the effects of 17-AAG seems to induce degradation of aberrantly expressed proteins, it is also possible and taken into account that 17-AAG could also induce degradation of prosurvival factors and play detrimental effects in cardiomyocytes.

In conclusion, our observations indicate that investigation of novel anti-p53 approach would open a way toward new treatment of myocardial infarction.

Acknowledgments

We thank Y. Ohtsuki, I. Sakamoto, M. Ikeda, and A. Furuyama for excellent technical support.

Sources of Funding

This work was supported by a Grant-in-Aid for Scientific Research on Priority Areas and for Exploratory Research (Ministry of Education, Culture, Sports, Science and Technology), Health and Labour Sciences Research grants (to I.K.), and research fellowships from the Japan Society for the Promotion of Science for Young Scientists (to A.T.N.). A.T.N. is a research fellow of the Japan Society for the Promotion of Science.

Disclosures

None.

References

1. Rosamond W, Flegal K, Friday G, Furie K, Go A, Greenlund K, Haase N, Ho M, Howard V, Kissela B, Kittner S, Lloyd-Jones D, McDermott M, Meigs J, Moy C, Nichol G, O'Donnell CJ, Roger V, Rumsfeld J, Sorlie P, Steinberger J, Thom T, Wasserthiel-Smoller S, Hong Y. Heart disease and stroke statistics–2007 update: a report from the American Heart Association Statistics Committee and Stroke Statistics Subcommittee. *Circulation*. 2007;115:e69–e171.
2. Kajstura J, Cheng W, Reiss K, Clark WA, Sonnenblick EH, Krajewski S, Reed JC, Olivetti G, Anversa P. Apoptotic and necrotic myocyte cell deaths are independent contributing variables of infarct size in rats. *Lab Invest*. 1996;74:86–107.
3. Wencker D, Chandra M, Nguyen K, Miao W, Garantziotis S, Factor SM, Shirani J, Armstrong RC, Kitsis RN. A mechanistic role for cardiac myocyte apoptosis in heart failure. *J Clin Invest*. 2003;111:1497–1504.
4. Haunstetter A, Izumo S. Toward antiapoptosis as a new treatment modality. *Circ Res*. 2000;86:371–376.
5. Chatterjee S, Stewart AS, Bish LT, Jayasankar V, Kim EM, Pirolli T, Burdick J, Woo YJ, Gardner TJ, Sweeney HL. Viral gene transfer of the antiapoptotic factor Bcl-2 protects against chronic postischemic heart failure. *Circulation*. 2002;106:I212–I217.
6. Hochhauser E, Kivity S, Offen D, Maulik N, Otani H, Barhum Y, Pannet H, Shneyvays V, Shainberg A, Goldshtaub V, Tobar A, Vidne BA. Bax ablation protects against myocardial ischemia-reperfusion injury in transgenic mice. *Am J Physiol Heart Circ Physiol*. 2003;284:H2351–H2359.
7. Imahashi K, Schneider MD, Steenbergen C, Murphy E. Transgenic expression of Bcl-2 modulates energy metabolism, prevents cytosolic acidification during ischemia, and reduces ischemia/reperfusion injury. *Circ Res*. 2004;95:734–741.
8. Hochhauser E, Cheporko Y, Yasovich N, Pinchas L, Offen D, Barhum Y, Pannet H, Tobar A, Vidne BA, Birk E. Bax deficiency reduces infarct size and improves long-term function after myocardial infarction. *Cell Biochem Biophys*. 2007;47:11–20.
9. Vogelstein B, Lane D, Levine AJ. Surfing the p53 network. *Nature*. 2000;408:307–310.
10. Haupt Y, Maya R, Kazaz A, Oren M. Mdm2 promotes the rapid degradation of p53. *Nature*. 1997;387:296–299.
11. Kubbutat MH, Jones SN, Vousden KH. Regulation of p53 stability by Mdm2. *Nature*. 1997;387:299–303.
12. Dornan D, Wertz I, Shimizu H, Arnott D, Frantz GD, Dowd P, O'Rourke K, Koeppen H, Dixit VM. The ubiquitin ligase COP1 is a critical negative regulator of p53. *Nature*. 2004;429:86–92.
13. Leng RP, Lin Y, Ma W, Wu H, Lemmers B, Chung S, Parant JM, Lozano G, Hakem R, Benchimol S. Pirh2, a p53-induced ubiquitin-protein ligase, promotes p53 degradation. *Cell*. 2003;112:779–791.
14. Long X, Boluyt MO, Hipolito ML, Lundberg MS, Zheng JS, O'Neill L, Cirielli C, Lakatta EG, Crow MT. p53 and the hypoxia-induced apoptosis

of cultured neonatal rat cardiac myocytes. *J Clin Invest.* 1997;99: 2635–2643.
15. Liu P, Xu B, Cavalieri TA, Hock CE. Pifithrin-alpha attenuates p53-mediated apoptosis and improves cardiac function in response to myocardial ischemia/reperfusion in aged rats. *Shock.* 2006;26:608–614.
16. Sano M, Minamino T, Toko H, Miyauchi H, Orimo M, Qin Y, Akazawa H, Tateno K, Kayama Y, Harada M, Shimizu I, Asahara T, Hamada H, Tomita S, Molkentin JD, Zou Y, Komuro I. p53-induced inhibition of Hif-1 causes cardiac dysfunction during pressure overload. *Nature.* 2007; 446:444–448.
17. Song K, Backs J, McAnally J, Qi X, Gerard RD, Richardson JA, Hill JA, Bassel-Duby R, Olson EN. The transcriptional coactivator CAMTA2 stimulates cardiac growth by opposing class II histone deacetylases. *Cell.* 2006;125:453–466.
18. Zou Y, Komuro I, Yamazaki T, Kudoh S, Uozumi H, Kadowaki T, Yazaki Y. Both Gs and Gi proteins are critically involved in isoproterenol-induced cardiomyocyte hypertrophy. *J Biol Chem.* 1999;274:9760–9770.
19. Sohal DS, Nghiem M, Crackower MA, Witt SA, Kimball TR, Tymitz KM, Penninger JM, Molkentin JD. Temporally regulated and tissue-specific gene manipulations in the adult and embryonic heart using a tamoxifen-inducible Cre protein. *Circ Res.* 2001;89:20–25.
20. Sahara N, Murayama M, Mizoroki T, Urushitani M, Imai Y, Takahashi R, Murata S, Tanaka K, Takashima A. In vivo evidence of CHIP up-regulation attenuating tau aggregation. *J Neurochem.* 2005;94:1254–1263.
21. Harada M, Qin Y, Takano H, Minamino T, Zou Y, Toko H, Ohtsuka M, Matsuura K, Sano M, Nishi J, Iwanaga K, Akazawa H, Kunieda T, Zhu W, Hasegawa H, Kunisada K, Nagai T, Nakaya H, Yamauchi-Takihara K, Komuro I. G-CSF prevents cardiac remodeling after myocardial infarction by activating the Jak-Stat pathway in cardiomyocytes. *Nat Med.* 2005;11:305–311.
22. McDonough H, Patterson C. CHIP: a link between the chaperone and proteasome systems. *Cell Stress Chaperones.* 2003;8:303–308.
23. Esser C, Scheffner M, Hohfeld J. The chaperone-associated ubiquitin ligase CHIP is able to target p53 for proteasomal degradation. *J Biol Chem.* 2005;280:27443–27448.
24. Tripathi V, Ali A, Bhat R, Pati U. CHIP chaperones wild type p53 tumor suppressor protein. *J Biol Chem.* 2007;282:28441–28454.
25. Graeber TG, Peterson JF, Tsai M, Monica K, Fornace AJ Jr, Giaccia AJ. Hypoxia induces accumulation of p53 protein, but activation of a G1-phase checkpoint by low-oxygen conditions is independent of p53 status. *Mol Cell Biol.* 1994;14:6264–6277.
26. An WG, Kanekal M, Simon MC, Maltepe E, Blagosklonny MV, Neckers LM. Stabilization of wild-type p53 by hypoxia-inducible factor 1alpha. *Nature.* 1998;392:405–408.
27. Chen KF, Lai YY, Sun HS, Tsai SJ. Transcriptional repression of human cad gene by hypoxia inducible factor-1alpha. *Nucleic Acids Res.* 2005; 33:5190–5198.
28. Eltzschig HK, Abdulla P, Hoffman E, Hamilton KE, Daniels D, Schonfeld C, Loffler M, Reyes G, Duszenko M, Karhausen J, Robinson A, Westerman KA, Coe IR, Colgan SP. HIF-1-dependent repression of equilibrative nucleoside transporter (ENT) in hypoxia. *J Exp Med.* 2005;202:1493–1505.
29. Ibla JC, Khoury J, Kong T, Robinson A, Colgan SP. Transcriptional repression of Na-K-2Cl cotransporter NKCC1 by hypoxia-inducible factor-1. *Am J Physiol Cell Physiol.* 2006;291:C282–C289.
30. Bindra RS, Glazer PM. Co-repression of mismatch repair gene expression by hypoxia in cancer cells: role of the Myc/Max network. *Cancer Lett.* 2007;252:93–103.
31. Waza M, Adachi H, Katsuno M, Minamiyama M, Sang C, Tanaka F, Inukai A, Doyu M, Sobue G. 17-AAG, an Hsp90 inhibitor, ameliorates polyglutamine-mediated motor neuron degeneration. *Nat Med.* 2005;11: 1088–1095.
32. Dickey CA, Kamal A, Lundgren K, Klosak N, Bailey RM, Dunmore J, Ash P, Shoraka S, Zlatkovic J, Eckman CB, Patterson C, Dickson DW, Nahman NS Jr, Hutton M, Burrows F, Petrucelli L. The high-affinity HSP90-CHIP complex recognizes and selectively degrades phosphorylated tau client proteins. *J Clin Invest.* 2007;117:648–658.
33. Suzuki K, Sawa Y, Kaneda Y, Ichikawa H, Shirakura R, Matsuda H. In vivo gene transfection with heat shock protein 70 enhances myocardial tolerance to ischemia-reperfusion injury in rat. *J Clin Invest.* 1997;99:1645–1650.
34. Sakamoto M, Minamino T, Toko H, Kayama Y, Zou Y, Sano M, Takaki E, Aoyagi T, Tojo K, Tajima N, Nakai A, Aburatani H, Komuro I. Upregulation of heat shock transcription factor 1 plays a critical role in adaptive cardiac hypertrophy. *Circ Res.* 2006;99:1411–1418.
35. Blagosklonny MV, An WG, Romanova LY, Trepel J, Fojo T, Neckers L. p53 inhibits hypoxia-inducible factor-stimulated transcription. *J Biol Chem.* 1998;273:11995–11998.
36. Chandrashekhar Y, Sen S, Anway R, Shuros A, Anand I. Long-term caspase inhibition ameliorates apoptosis, reduces myocardial troponin-I cleavage, protects left ventricular function, and attenuates remodeling in rats with myocardial infarction. *J Am Coll Cardiol.* 2004;43:295–301.
37. Balsam LB, Kofidis T, Robbins RC. Caspase-3 inhibition preserves myocardial geometry and long-term function after infarction. *J Surg Res.* 2005;124:194–200.
38. Crow MT, Mani K, Nam YJ, Kitsis RN. The mitochondrial death pathway and cardiac myocyte apoptosis. *Circ Res.* 2004;95:957–970.
39. Matsusaka H, Ide T, Matsushima S, Ikeuchi M, Kubota T, Sunagawa K, Kinugawa S, Tsutsui H. Targeted deletion of p53 prevents cardiac rupture after myocardial infarction in mice. *Cardiovasc Res.* 2006;70: 457–465.
40. Solit DB, Basso AD, Olshen AB, Scher HI, Rosen N. Inhibition of heat shock protein 90 function downregulates Akt kinase and sensitizes tumors to Taxol. *Cancer Res.* 2003;63:2139–2144.

Novelty and Significance

What Is Known?

- Inhibition of myocardial apoptosis after myocardial infarction is cardioprotective.
- p53 expression is increased after myocardial infarction and induces cardiomyocyte apoptosis.

What New Information Does This Article Contribute?

- We identified CHIP as the endogenous p53 antagonist expressed in the heart.
- We found that CHIP downregulation is critically involved in the molecular mechanisms for p53 elevation after myocardial infarction.
- We showed several possibilities of the anti-p53 treatment after myocardial infarction.

Accumulation of tumor suppressor protein p53 in the myocardium causes the transition from adaptive cardiac hypertrophy to heart failure. However, the mechanisms of p53 accumulation in the heart and its therapeutic implications have been elusive. Here we show that downregulation of the chaperone-associated E3 ubiquitin ligase CHIP (carboxyl terminus of Hsp70-interacting protein) mediates hypoxia-induced p53 accumulation in the heart and that promotion of CHIP-induced p53 degradation protects the heart from ischemic injury. Under physiological conditions, CHIP limited the p53 protein amount at low levels by inducing proteasomal degradation of p53. Under hypoxic conditions, hypoxia inducible factor-1 (HIF-1) downregulated CHIP, resulting in the accumulation of p53. Overexpression of CHIP or administration of an Hsp90 inhibitor promoted CHIP-mediated p53 degradation and attenuated ischemic cardiac injury. These results indicate that CHIP is a crucial negative regulator of p53 in the heart and suggest that promotion of CHIP-mediated p53 degradation could be a novel therapeutic strategy for heart diseases.

Detailed Methods

Expression Cloning.

Expression cloning was performed as described previously [1] using PG13-Luc (A kind gift from B. Vogelstein) as a reporter plasmid. Initially, cDNA expression library from human heart (Invitrogen) was separated into small pools that contain ~100 clones each. cDNA clones that downregulate PG13 activity were isolated by sib-selection.

Plasmids and Transfection assay.

Transfection into COS7 cells were performed using Fugene HD (Roche). HA-tag was introduced to the N-terminus of human CHIP using PCR and subcloned into pCAGGS vector [2]. Flag-tagged p53 was from B. Gellersen [3]. Adenoviral vector of HA-tagged CHIP was created using AdEasy Vector System (Qbiogen) and infected as described previously[4]. Human CHIP promotor (-329 to +39 from TSS) was cloned into pGL4-basic (Promega). Mutations of the HRE site (CACGTG to CTGGCG) were introduced using the QuickChange Site-Directed Mutagenesis Kit (Stratagene). Stealth siRNA against rat CHIP, MDM2, HIF-1α, and p53 were designed and purchased from Invitrogen. Sequences for each siRNAs are; rat CHIP-1: ugguguaguacacugccacaagugg; rat CHIP-2: cucaucauaacucuccaucucuagc; rat MDM2-1: agcuaaggaaauuucaggaucuccc; rat MDM2-2: auagucgucacucuccugugacagg; rat HIF1α: uagugcuuccaucagaaggacuugc; rat Tp53: uuaagggugaaauauucuccaucga. Negative controls for siRNA was purchased from Invitrogen (Medium GC). Transfection of siRNA was performed using Lipofectamine RNAiMax (Invitrogen).

Cell culture.

COS7 and HEK293 cells are from ATCC and cultured in DMEM containing 10% FBS (Invitrogen). Neonatal rat cardiomyocytes were isolated from 1-day old Wistar rats and

cultured as described previously [5]. Cardiomyocytes were exposed to hypoxic stress by culturing under $CoCl_2$ (250 μM) or by culturing in hypoxic chamber (<1% O_2, PO_2 18~20mmHg).

Evaluation of apoptosis

Caspase-3 activity was examined by using CaspACE™ Assay System, Colorimetric (Promega). Annexin V staining was performed as previously described [4] using Annexin V-Cy3 apoptosis detection kit (Bio Vision). TUNEL staining on fresh frozen section of the heart was performed using In situ apoptosis detection kit (TaKaRa) and fluorescence was enhanced using anti-fluorescein rabbit IgG Alexa488 conjugated (Molecular Probe). The section was counterstained with α-sarcomeric actinin (SantaCruz) and DAPI. We have performed TUNEL staining 24 hours after coronary artery ligation because myocardial apoptosis was most prominent 24 hours after the operation (unpublished observations).

Luciferase assays

The reporter plasmid, PG13-Luc, pGL4-CHIP, or pGL4-CHIP-mutHRE was transfected into COS7 cells using Fugene HD (Roche) or to neonatal rat cardiomyocytes using Lipofectamine 2000 (Invitrogen). pRL-tk encoding Renilla luciferase was co-transfected as an internal control. Luciferase assay was carried out 24 hours after transfection of the effector plasmids or addition of drugs using dual-luciferase assay system (Promega).

RNA analysis

Total RNA extraction and DNase treatment was performed using SV total RNA isolation Kit (Promega). RNA was DNase treated and reverse transcribed using QuantiTect Reverse Transcription Kit (QIAGEN). Real time quantitative PCR was performed using

Universal Probe Library (UPL) (Roche) and Light Cycler TaqMan Master kit (Roche). Relative levels of gene expression were normalized to the rat GAPDH (for rat cardiomyocytes) or human β-actin (for HEK293 cells) expression using the comparative Ct method according to the manufacturer's instructions. Primer sequences and UPL number were; rat GAPDH: Fwd aatgtatccgttgtggatctga, Rev gcttcaccaccttcttgatgt and UPL No. 80; Human beta actin: Fwd ggaaatcgtgcgtgacatta, Rev ccgtcaggcagctcgtag and UPL No. 80; rat CHIP: Fwd ctcaaggagcagggaaacc, Rev aagtgggttccgggtgat and UPL No. 70; human p21: Fwd cgaagtcagttccttgtggag, Rev catgggttctgacggacat and UPL No. 82; human PUMA: Fwd gacctcaacgcacagtacga, Rev gagattgtacaggaccctcca and UPL No. 68; human MDM2: Fwd tctgatagtatttccctttcctttg, Rev tgttcacttacaccagcatcaa and UPL No. 21.

Protein analysis.

Whole cell lysates (50-100 μg) were separated by SDS-PAGE. Proteins were transferred to polyvinylidene difluoride membrane and incubated with primary antibodies followed by incubation with a HRP-conjugated secondary antibody (Jackson). Membrane was developed using ECL-Plus (Amersham). Densitometric analysis for the band intensity was performed using ImageJ. Immunoprecipitation was performed using specific antibodies and Protein A/G agarose (SantaCruz). Antibodies used were; anti-CHIP (CHEMICON), anti-p53 (1C12) (Cell Signaling), anti-HA (Roche), anti-Flag (M2) (Sigma), anti-MDM2 (R&D), anti-ubiquitin (CHEMICON), anti-HIF-1α (Novus), anti-PARP (Cell signaling), and anti-actin (Sigma).

HIF-1α activity was determined using TransAM™ HIF-1 (ActiveMotif).

Animals

All protocols were approved by Chiba University review board. CHIP heterozygous mice

and cardiac-specific inducible HIF-1 knockout mice were described [6-8]. Unlike the CHIP-deficient mice described by Dai et al. [9], our CHIP heterozygous mice were maintained on a pure C57BL/6 background. Very few homozygous knockout were obtained (2.9% of the alive embryo) but all of them were small in size and died before 1 week after birth. The reason for perinatal lethality in our mouse strain remains to be elucidated. Cardiac-specific CHIP transgenic mice were generated by pronuclear injection of αMHC-HA-CHIP transgene construct. Two independent lines that express HA-tagged CHIP to the same level were obtained and both lines showed similar results. Cardiac specific expression of HA-tagged CHIP was confirmed by Western blotting. The basal cardiac parameters of the mice used in this study (CHIP heterozygous knockout mice and cardiac specific CHIP overexpressing transgenic mice) were shown in Table 1. Permanent coronary artery ligation was performed on 10-week old male mice as described previously [4]. We anesthetized mice by intraperitoneally injecting a mixture of 100 mg/kg ketamine and 5 mg/kg xylazine. 17-AAG (Alexis) was dissolved in DMSO and injected intraperitoneally right after coronary artery ligation.

Physiological analysis and histological analysis.

Echocardiography was performed as described previously [8]. Paraffin-embedded heart samples were sectioned and stained with Masson's Trichrome staining as previously described [4].

Statistical analysis.

Data are expressed as mean±SE. The significance of differences among means was evaluated using analysis of variance (ANOVA), followed by Fisher's PLSD test and Dunnett's test for multiple comparisons. Significant differences were defined as $P<0.05$.

Supplemental References

1. Song K, Backs J, McAnally J, Qi X, Gerard RD, Richardson JA, Hill JA, Bassel-Duby R, Olson EN. The transcriptional coactivator CAMTA2 stimulates cardiac growth by opposing class II histone deacetylases. *Cell.* 2006;125:453-466.
2. Akazawa H, Kudoh S, Mochizuki N, Takekoshi N, Takano H, Nagai T, Komuro I. A novel LIM protein Cal promotes cardiac differentiation by association with CSX/NKX2-5. *J Cell Biol.* 2004;164:395-405.
3. Schneider-Merck T, Pohnke Y, Kempf R, Christian M, Brosens JJ, Gellersen B. Physical interaction and mutual transrepression between CCAAT/enhancer-binding protein beta and the p53 tumor suppressor. *J Biol Chem.* 2006;281:269-278.
4. Harada M, Qin Y, Takano H, Minamino T, Zou Y, Toko H, Ohtsuka M, Matsuura K, Sano M, Nishi J, Iwanaga K, Akazawa H, Kunieda T, Zhu W, Hasegawa H, Kunisada K, Nagai T, Nakaya H, Yamauchi-Takihara K, Komuro I. G-CSF prevents cardiac remodeling after myocardial infarction by activating the Jak-Stat pathway in cardiomyocytes. *Nat Med.* 2005;11:305-311.
5. Zou Y, Komuro I, Yamazaki T, Kudoh S, Uozumi H, Kadowaki T, Yazaki Y. Both Gs and Gi proteins are critically involved in isoproterenol-induced cardiomyocyte hypertrophy. *J Biol Chem.* 1999;274:9760-9770.
6. Sohal DS, Nghiem M, Crackower MA, Witt SA, Kimball TR, Tymitz KM, Penninger JM, Molkentin JD. Temporally regulated and tissue-specific gene manipulations in the adult and embryonic heart using a tamoxifen-inducible Cre protein. *Circ Res.* 2001;89:20-25.
7. Sahara N, Murayama M, Mizoroki T, Urushitani M, Imai Y, Takahashi R, Murata S, Tanaka K, Takashima A. In vivo evidence of CHIP up-regulation attenuating tau aggregation. *J Neurochem.* 2005;94:1254-1263.
8. Sano M, Minamino T, Toko H, Miyauchi H, Orimo M, Qin Y, Akazawa H, Tateno K, Kayama Y, Harada M, Shimizu I, Asahara T, Hamada H, Tomita S, Molkentin JD, Zou Y, Komuro I. p53-induced inhibition of Hif-1 causes cardiac dysfunction during pressure overload. *Nature.* 2007;446:444-448.
9. Dai Q, Zhang C, Wu Y, McDonough H, Whaley RA, Godfrey V, Li HH, Madamanchi N, Xu W, Neckers L, Cyr D, Patterson C. CHIP activates HSF1 and confers protection against apoptosis and cellular stress. *Embo J.* 2003;22:5446-5458.

Online Figure I

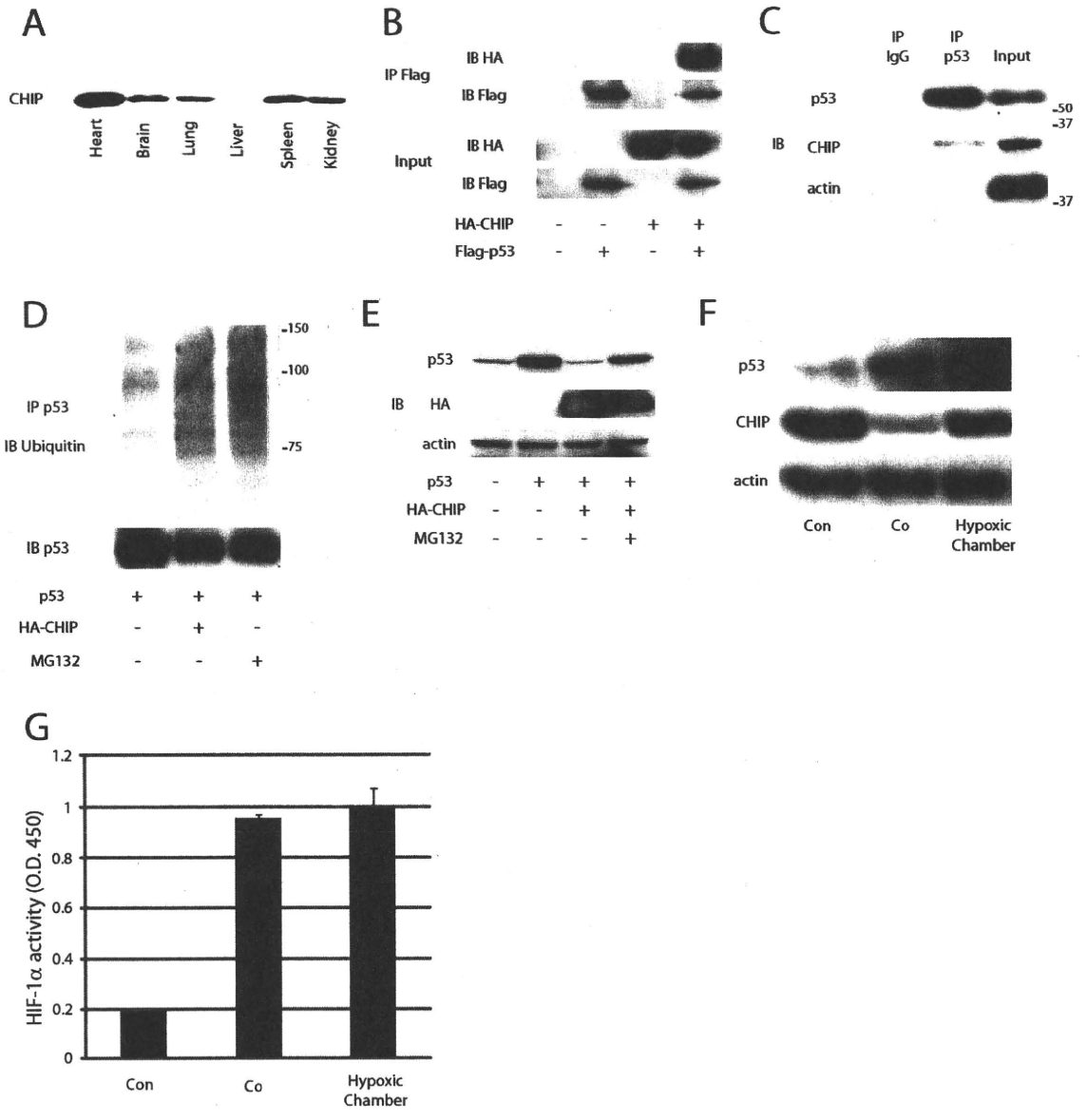

Online Figure II

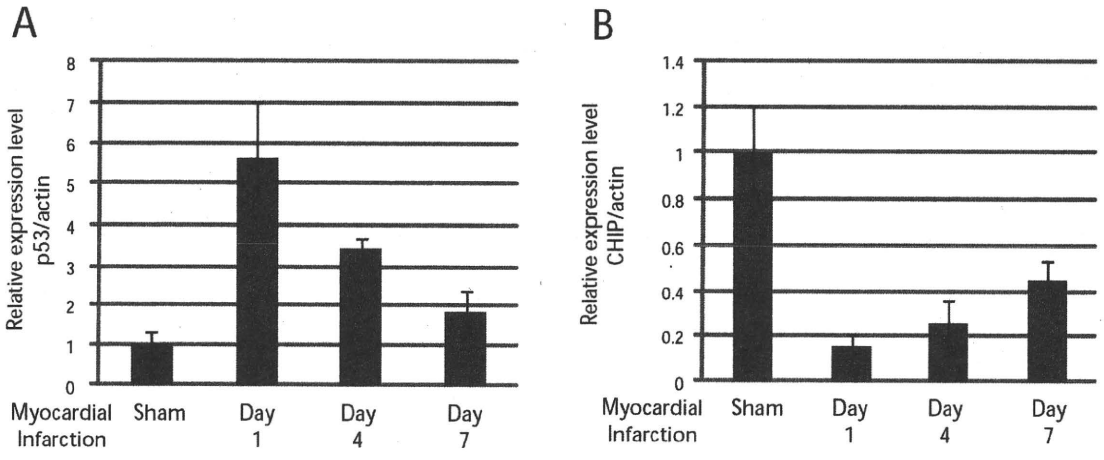

Online Figure III

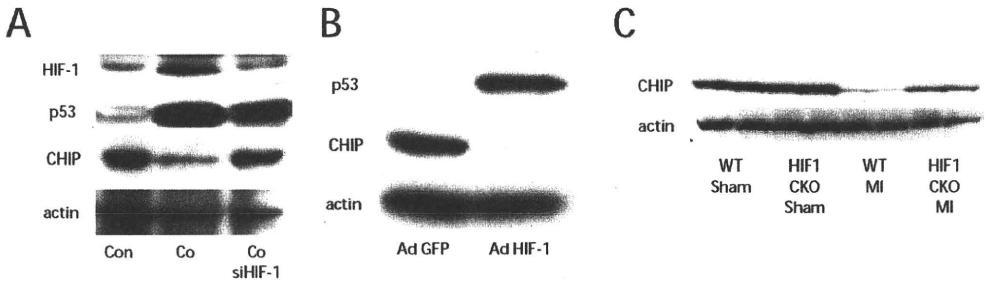

Online Figure IV

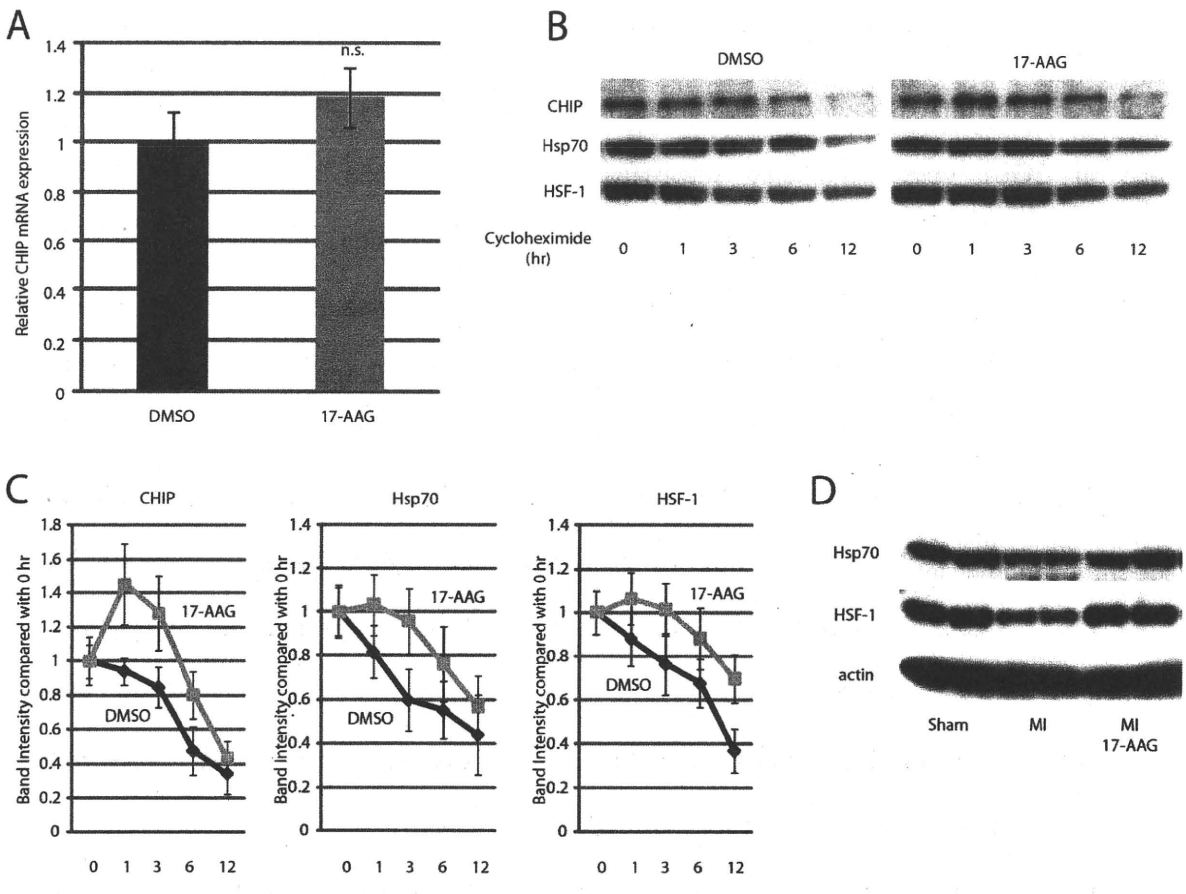

Figure Legends for Supplementary Figures

Online Figure I. (**A**) Tissue distribution of endogenous CHIP. (**B**) CHIP interacts with p53 in COS7 cells transfected with HA-CHIP and Flag-p53 as revealed by immunoprecipitation/western blot analysis. IP, immunoprecipitation. (**C**) Endogenous CHIP interacts with endogenous p53 in neonatal rat cardiomyocytes. (**D**) CHIP induces ubiquitination of p53 in cultured cardiomyocytes. Ubiquitinated p53 appears as a smear. MG132 was used as a positive control because it inhibits proteasomal degradation, leaving ubiquitinated protein undegraded. (**E**) MG132 prevents CHIP-induced p53 degradation in cultured cardiomyocytes. (**F**) Both $CoCl_2$ treatment and hypoxia induces p53 upregulation and CHIP downregulation in cardiomyocytes. Con, control; Co, $CoCl_2$. (**G**) HIF-1α activity was determined to confirm that HIF-1α was actually active by $CoCl_2$ treatment. Con, control; Co, $CoCl_2$.

Online Figure II. Densitometric analysis for the Western blot shown in Figure 2B. p53 protein level (**A**), and CHIP protein level (**B**).

Online Figure III. (**A**) Knockdown of HIF-1α by siRNA reverses the effect of $CoCl_2$ in cardiomyocytes. (**B**) Overexpression of HIF-1 downregulates CHIP expression and induces accumulation of p53 in cardiomyocytes. (**C**) Wild type and cardiac-specific inducible HIF-1α knockout mice were subjected to coronary artery ligation. HIF-1 deletion attenuates downregulation of CHIP expression induced by myocardial infarction. WT, wild type mice; CKO, cardiac-specific inducible HIF-1α knockout mice.

Online Figure IV. (**A**) 17-AAG treatment showed no effect on CHIP mRNA transcription. (**B**) Representative blots for the expression level of CHIP, Hsp70 and HSF-1 after treatment with cycloheximide 100 μg/mL, with or without 17-AAG. (**C**) Kinetics of protein stability obtained from densitometric analysis. (**D**) 17-AAG treatment up-regulates the protein level of Hsp70 and HSF-1 after myocardial infarction.

Current Alzheimer Research, 2010, 7, 665-669

TAU Aggregation is a Therapeutic Target for Alzheimer's Disease

A. Takashima*

Laboratory for Alzheimer's disease, Brain Science Institute, RIKEN; 2-1 Hirosawa, Wako-shi, Saitama 351-0198, Japan

Abstract: Based on the amyloid hypothesis, studies for AD therapy have been mostly focused on removing β-amyloid. Recent results of amyloid immunotherapy raised the question whether β-amyloid is sufficient target for AD therapy. Neurofibrillary tangles (NFTs), which contain hyperphosphorylated tau, are another pathological hallmark of AD. NFTs are observed in entorhinal cortex, limbic, and neocortex over the course of clinical progression. NFTs are associated with synapse and neuron loss, suggesting that the process of NFT formation is involved in brain dysfunction. During NFT formation, tau forms a variety of different aggregation species, including tau oligomers, granules, and fibrils. Analysis of different human tau-expressing mouse lines reveals that soluble hyperphosphorylated tau, which includes tau oligomer, is involved in synapse loss, whereas granular tau formation is involved in neuronal loss. Therefore, inhibition of tau aggregation and tau phosphorylation is expected to prevent synapse loss and neuron loss, and may slow or halt the progressive dementia in AD.

Keywords: Oligomer tau, granular tau, synapse loss, neuron loss.

β-AMYLOID HYPOTHESIS

The two major pathological features of AD are senile plaques (SPs), which are β-amyloid deposits (Aβ) in the extracellular space, and neurofibrillary tangles (NFT), which are intraneuronal inclusions of hyperphosphorylated tau. The composition of SPs and NFTs suggested that Aβ and tau are involved in development of AD. Mutations in amyloid precursor protein (APP) induce AD with 100% penetration, and familial Alzheimer's disease (FAD)-associated mutations of APP lead to an increased level of Aβ generation or Aβ aggregation; these findings support the β-amyloid hypothesis [1-4]. Studies of other causative genes for FAD, presenilin 1 and 2, further support the β-amyloid hypothesis. The presenilin 1 and 2 genes are located on chromosome 14 and 1, and their gene products are membrane proteins with membrane-spanning regions that localize to the nuclear membrane, endoplasmic membrane, and plasma membrane in regions of cell-cell adhesion [5-7]. PS1 mutations are associated with an increased ratio of secreted Aβ42/Aβ40 [8]. PS1 is a component of the γ-secretase complex[9,10], and FAD-associated mutations in PS1 reduce γ-secretase activity. This dysfunction of γ-secretase has a greater effect on generation of Aβ40 than Aβ42, leading to an increased Aβ42/Aβ40 ratio, with an overall reduction in total Aβ generation. The increased Aβ42/Aβ40 ratio results in more toxic Aβ aggregation, suggesting that the level of Aβ aggregate, rather than the total Aβ level, is the important factor in development of AD. Indeed, aggregated Aβ caused neurotoxicity in cultured primary neurons, strongly supporting the β-amyloid hypothesis. Primary neurons from tau deficient mouse did not exhibit Aβ-induced neurotoxicity, indicating that Aβ-induced neurotoxicity requires tau [11]. However, the APP-overexpressing mouse (APP-Tg) exhibits Aβ deposition and memory impairment without NFTs and neuronal loss. This partially supports the β-amyloid hypothesis.

In Aβ immunotherapy, immunizing a mouse against Aβ42 prevents Aβ deposition and memory impairment [12-17], suggesting that Aβ immunotherapy can remove Aβ oligomers, believed to be a cause of memory deficits. Clinical trials of the immunization in AD patients, however, did not show the same results as in the mouse model. While immunotherapy resulted in the removal of Aβ plaques in AD brains, the removal of plaques failed to halt progressive neurodegeneration [18]. There are several reasons why Aβ immunotherapy might have been ineffective in treating AD patients. However, just because Aβ immunotherapy was ineffective in treating AD patients, we cannot conclude that Aβ does not play a role in AD. Indeed, all of the causative genes for FAD affect Aβ generation, and Aβ oligomers induce synaptic dysfunction the in brain, strongly suggesting that Aβ does indeed play some role in AD neuropathology. APP-overexpressing mice do exhibit memory impairment without tau pathology or neuronal loss, whereas reduction of tau levels in APP-overexpressing mice prevent Aβ-induced memory deficits [19]; therefore, some changes in tau prior to NFT formation may be involved in memory impairment. However, these changes in tau may be insufficient to cause NFT formation and neuronal loss. Therefore, pathological changes in tau, which lead to NFT formation and neuronal loss, may be key to understanding why Aβ removal fails to halt the clinical course of AD in humans.

RELATIONSHIP BETWEEN PATHOLOGICAL CHANGES AND CLINICAL DEVELOPMENT OF AD

The progression of AD symptoms varies in each individual. However, in early stages, symptoms are usually similar.

*Address correspondence to this author at the Laboratory for Alzheimer's Disease, Brain Science Institute, RIKEN; 2-1 Hirosawa, Wako-shi, Saitama 351-0198; Japan; Tel:/Fax: 048-467-9704
E-mail: kenneth@brain.riken.go.jp

1567-2050/10 $55.00+.00

According to the Global Deterioration Scale (GDS)[20], in the case of no cognitive decline (Stage 1), individuals have no problems in daily living. In very mild cognitive decline (Stage 2), individuals forget names and locations of objects, and may have trouble finding words. These behaviors are dependent on functions of the entorhinal cortex/ hippocampus, and parts of the prefrontal cortex. In mild cognitive decline (Stage 3), individuals face difficulty in traveling to new locations and handling problems at work, neural functions that also depend on entorhinal cortex/hippocampus, and parts of the prefrontal cortex. In moderate cognitive decline (Stage 4), individuals have difficulty with complex tasks, a function that depends on the prefrontal cortex. From moderately severe cognitive decline to very severe cognitive decline (Stages 5 to 7), in addition to dysfunctions associated with entorhinal cortex/hippocampus and prefrontal cortex, individuals require help with daily living; these functions are associated with basal ganglia, amygdala, and association cortexes. Thus, abilities of memory formation and recall, which relate to functions of entorhinal cortex/hippocampus, and prefrontal cortex, are first impaired in the early cognitive decline stage; subsequently, the impairment spreads to other areas of the brain, leading to dementia.

In Braak stage I, NFTs are formed in transentorhinal cortex and the CA1 region of the hippocampus. The number of NFTs increases in Braak stage II; Braak stages I and II together are called the transentorhinal stage. Braak stages I and II are classified as normal aging. In Braak stages III and IV, called the limbic stage, many ghost tangles appear in the entorhinal cortex, and NFTs are found throughout the entire limbic system, in hippocampal regions CA1–4 and amygdala. In the limbic stage, patients show various AD-specific symptoms, such as memory impairment, reduced spatial cognition, and reduced desire, as a result of neural dysfunction in the limbic system. In Braak stages V and VI, called the isocortical stage, NFTs are present, and neural function in the cerebral cortex is impaired, causing dementia. This increasing extent of NFTs correlates with increasing impairment of brain function. The number of NFTs in CA1, subiculum, and CA4 of the hippocampal formation correlates with the degree of dementia, and synapse loss in dentate gyrus, CA2/3, and CA4 strongly correlates with the degree of dementia [21]. Therefore, the distribution of NFTs correlates with disease progression in Alzheimer's disease (AD), and synapse loss may be key to understanding dementia in AD.

NFT FORMATION AND NEURONAL DYSFUNCTION

Tauopathies are a class of neurodegenerative diseases stemming from the pathological aggregation of tau protein, which is called neurofibrillary tangle (NFT) in the human brain. NFT is observed in a wide range of age-related neurodegenerative diseases, such as Alzheimer's disease, Pick disease (PiD), Progressive supranuclear palsy (PSP), and corticobasal degeneration. Because all NFT-related diseases are accompanied by neurological disorders due to neuronal dysfunction, NFT is considered to be a common pathological marker for neurological disorders. The rate of neuronal loss is much higher than that of NFTs, suggesting that there may be a common mechanism between NFT formation and neuron death [22, 23]. This hypothesis is strongly supported by the discovery of a tau gene mutation in frontotemporal dementia with parkinsonism linked to chromosome 17 (FTDP-17) [24-26], a dementing disease associated with NFT formation and neuronal loss. The elucidation of mutated tau in FTDP-17 conclusively demonstrated that tau dysfunction or abnormality alone can induce neurodegeneration characterized by NFTs and neuronal death and leading to clinical dementia.

An FTDP-17 mouse model that displays age-related NFTs, neuronal death, and behavioral deficits may shed light on the issue of how tau induces neuronal dysfunction. These mice overexpress P301L mutant tau under the regulation of a tetracycline-inducible promoter. Although inhibiting mutant tau overexpression in these mice blocks neuronal death and improves memory, NFTs continue to form [27], indicating that NFTs may not be responsible for neuronal death. Recent observations that NFT-bearing neurons contained activated caspase but did not undergo acute apoptosis [28] suggest that NFTs are not themselves toxic, but that instead the mechanism of NFT formation is shared by the processes underlying neuronal death and neuronal dysfunction. The relationship between neuronal loss and memory dysfunction in the P301L mutant tau mouse model remains unclear. However, an examination of NFT formation may reveal the key to understanding tau-induced neuronal dysfunction.

PROCESS OF NFT FORMATION FROM MONOMERIC TAU

NFTs consist of two aggregated tau species, PHFs (Paired helical filaments) and SFs (Straight filaments). The mechanism of tau fibril formation is not fully understood, due to technical difficulties involved in electron microscopic observations of these fibers. However, tau fibril formation has been studied extensively *in vitro*. Anionic surfactants accelerate fibril formation of tau protein *in vitro* [29], and fibril formation can then be monitored by thioflavin (ThT) fluorescence, which recognizes protein aggregations with a β-sheet conformation. To track structural changes in tau in solution, and to understand the relationship between different tau aggregates, we investigated how tau assembly *in vitro* changes over time, by measuring ThT fluorescence and using atomic force microscopy (AFM) [30].

Before ThT fluorescence can be detected, tau forms oligomers (dimers to octamers) as incubation time increases [31]. Although these tau oligomers could not be observed under AFM, they were detected by SDS-PAGE performed under non-reducing conditions. Under reducing conditions, however, tau oligomers consisting of three or more tau molecules were no longer detected, suggesting that tau oligomers form through disulfide bonds and other SDS-resistant tau-tau associations. As ThT fluorescence increases, two forms of tau aggregates can be observed with AFM: a granular tau aggregate and a fibrillar tau aggregate. Laser light scattering analysis of sucrose-gradient purified granular tau aggregates indicated that a single granular tau aggregate consists of about 40 tau molecules. Since an increased concentration of granular tau aggregate induces the formation of tau fibrils, granular tau has been proposed to be an intermediate form of tau fibrils [30]. As shown in Fig. (**1**) monomeric tau first binds together through disulfide bonds and SDS-

resistant interactions to form tau oligomers, which are not visible under AFM. Forty tau molecules bind together forming a β-sheet structure. These 40-tau aggregates appear granular in shape under AFM. Accumulations of granular tau stick together to form tau fibrils. Therefore, before tau fibrils are formed, tau forms two different types of aggregates: tau oligomers, which are not detectable by ThT staining or by AFM, and granular tau oligomers.

ROLE OF TAU AGGREGATIONS IN SYNAPSE LOSS AND NEURON LOSS SEEN IN AD

To understand tau-induced brain dysfunction in neurodegenerative disease and aging, we generated a transgenic mouse line expressing wild-type human tau. These mice exhibit impaired place learning and memory, but neither NFT formation nor neuronal loss at old age. To determine which brain region's activity is linked to impairment of place learning in this mouse model, we analyzed the relationship between age-dependent tau-induced changes in behavior and the corresponding activity in all brain regions, using Mn-enhanced MRI (MEM) methods. MEM showed that activity in the parahippocampal area strongly correlates with a decline in memory, as assessed by the Morris water maze. In these mice, hyperphosphorylated tau and synapse loss were found in the same brains regions that also show hyperphosphorylated tau and synapse loss with normal aging. Taken together, the accumulation of hyperphosphorylated tau in aged mice, leading to inhibition of neural activity due to synapse loss in parahippocampal areas including the entorhinal cortex, may underlie place learning impairment. Thus, the accumulation of hyperphosphorylated tau that occurs before NFT formation in entorhinal cortex may contribute to the memory problems seen in AD.

Expression of FTDP-17 mutant tau in mouse brain induces neuronal loss and NFT formation. Biochemical analysis indicated that mice expressing FTDP-17 mutant tau form a sarcosyl-insoluble tau aggregation concomitant with neuronal loss and NFT formation. Because insoluble tau includes fibrillar and granular tau aggregations, and NFTs themselves are not the toxic tau species, we speculate that the granular tau oligomer may be involved in neuronal loss. The report that the inhibiting mutant tau overexpression in mice overexpressing P301L mutant tau under the regulation of a tetracycline-inducible promoter [27] blocked neuronal loss, but remained NFT formation could be explained by following, if granular tau oligomer is a toxic tau aggregation, and fibril does not have toxicity. The inhibition of tau expression reduces new formation of granular tau oligomer,

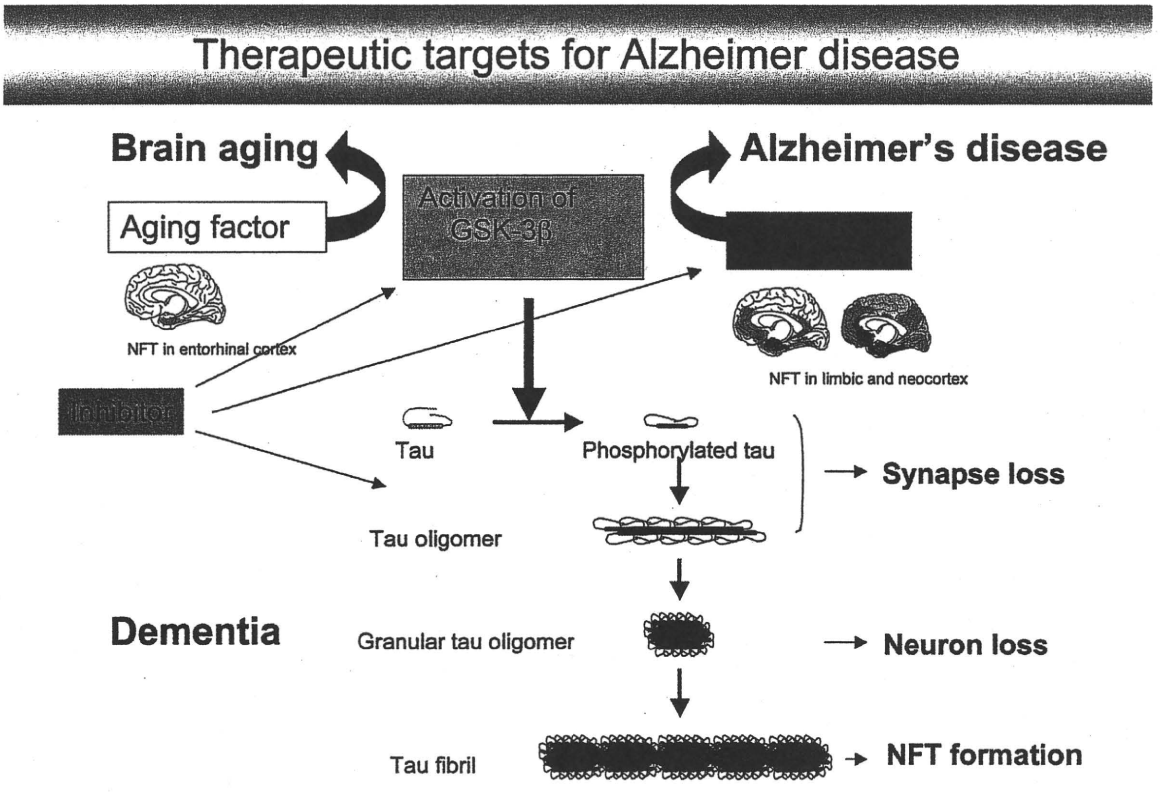

Fig. (1). An aging-related factor activates GSK-3b. Activation of GSK-3b induces hyperphosphorylated tau, leading to formation of NFTs in entorhinal cortex. During NFT formation, neuron loss and synapse loss occur in entorhinal cortex, resulting in memory loss. In AD, Aβ accelerates, spreading NFTs from entorhinal cortex to limbic and neocortex by activation of GSK-3β. During NFT formation, neuron loss and synapse loss occur in limbic cortex and neocortex, leading to dementia. Hyperphosphorylated tau is dislodged from microtubules because it has a greater affinity for tau-tau interaction. Hyperphosphorylated tau binds together and forms oligomeric tau, which is still detergent-soluble and cannot be detected under AFM. Both hyperphosphorylated tau by itself and oligomeric tau are involved in synaptic loss, as observed in the wild human tau Tg mouse. When oligomeric tau consists of ~40 molecules, possesses a β-sheet structure, and forms a granular shape under AFM, it becomes a detergent-insoluble aggregate. This granular tau oligomer may be involved in neuronal loss.

leading to a blockade of the neuronal death cascade. The pre-existing granular tau oligomers stick together and form tau fibrils, which may be non-toxic, resulting in a blockade of neuron loss by reducing the concentration of granular tau oligomer.

As shown in Fig. (1) hyperphosphorylated tau is dislodged from microtubules because it has a greater affinity for tau-tau interaction. Hyperphosphorylated tau molecules bind together, and form oligomeric tau, which is still soluble in detergent, and cannot be detected under AFM. Both hyperphosphorylated tau and oligomeric tau are involved in synaptic loss, as observed in the wild human tau Tg mouse. When oligomeric tau consists of ~40 molecules, possesses a β-sheet structure, and forms a granular shape under AFM, it becomes a detergent-insoluble aggregate. This granular tau oligomer may be involved in neuronal loss. The granular tau oligomer fuses together, and forms tau fibrils, resulting in NFT formation. Thus, in tauopathies, different forms of tau aggregation are involved in different pathological changes. The underlying each mechanism may be in common with the other neurodegenerative disease accompanying with intracellular protein inclusion. Therefore, in cases of tauopathy including AD, tau changes are the cause of neural dysfunction due to synapse loss and neuronal loss.

CONCLUSION

Based on the study of Braak stages, NFTs are observed in entorhinal cortex before Aβ deposition, and then spread into limbic cortex and neocortex after Aβ deposition. An aging-related factor and Aβ may be the cause of NFT formation in entorhinal cortex, limbic cortex, and neocortex. In either case, during NFT formation, synapse loss and neuron loss occur, and brain function is consequently impaired in the region where NFTs are formed. Therefore, inhibition of tau aggregation and tau phosphorylation is expected to prevent synapse loss and neuron loss in AD.

REFERENCES

[1] M. Citron T, Oltersdorf C, Haass L, McConlogue AY, Hung P, Seubert C, *et al.* Mutation of the beta-amyloid precursor protein in familial Alzheimer's disease increases beta-protein production. Nature 360: 672-4 (1992).

[2] Felsenstein KM, Hunihan LW, Roberts SB. Altered cleavage and secretion of a recombinant beta-APP bearing the Swedish familial Alzheimer's disease mutation. Nat Genet 6: 251-5 (1994).

[3] Goate A, Chartier-Harlin MC, Mullan M, Brown J, Crawford F, Fidani L, *et al.* Segregation of a missense mutation in the amyloid precursor protein gene with familial Alzheimer's disease. Nature 349: 704-6 (1991).

[4] Hardy J, Allsop D. Amyloid deposition as the central event in the aetiology of Alzheimer's disease. Trends Pharmacol Sci Vol. 12, pp. 383-8 (1991).

[5] Rogaev EI, Sherrington R, Rogaeva EA, Levesque G, Ikeda M, Liang Y, *et al.* Familial Alzheimer's disease in kindreds with missense mutations in a gene on chromosome 1 related to the Alzheimer's disease type 3 gene. Nature 376: 775-8 (1995).

[6] Sherrington R, Rogaev EI, Liang Y, Rogaeva EA, Levesque G, Ikeda M, *et al.* Cloning of a gene bearing missense mutations in early-onset familial Alzheimer's disease. Nature 375: 754-60 (1995).

[7] Takashima A, Sato M, Mercken M, Tanaka S, Kondo S, Honda T, *et al.* Localization of Alzheimer-associated presenilin 1 in transfected COS-7 cells. Biochem Biophys Res Commun 227: 423-6 (1996).

[8] Murayama O, Tomita T, Nihonmatsu N, Murayama M, Sun X, Honda T, *et al.* Enhancement of amyloid beta 42 secretion by 28 different presenilin 1 mutations of familial Alzheimer's disease. Neurosci Lett 265: 61-3 (1999).

[9] Edbauer D, Winkler E, Regula JT, Pesold B, Steiner H, Haass C. Reconstitution of gamma-secretase activity. Nat Cell Biol 5: 486-8 (2003).

[10] Takasugi N, Tomita T, Hayashi I, Tsuruoka M, Niimura M, Takahashi Y, *et al.* The role of presenilin cofactors in the gamma-secretase complex. Nature 422: 438-41 (2003).

[11] Rapoport M, Dawson HN, Binder LI, Vitek MP, Ferreira A. Tau is essential to beta -amyloid-induced neurotoxicity. Proc Natl Acad Sci USA 99: 6364-9 (2002).

[12] Chapman PF. Alzheimer's disease: model behaviour. Nature 408: 915-6 (2000).

[13] Dodart JC, Bales KR, Gannon KS, Greene SJ, DeMattos RB, Mathis C, *et al.* Immunization reverses memory deficits without reducing brain Abeta burden in Alzheimer's disease model. Nat Neurosci 5: 452-7 (2002).

[14] Klyubin I, Walsh DM, Lemere CA, Cullen WK, Shankar GM, Betts V, *et al.* Amyloid beta protein immunotherapy neutralizes Abeta oligomers that disrupt synaptic plasticity *in vivo*. Nat Med 11: 556-61 (2005).

[15] McLaurin J, Cecal R, Kierstead ME, Tian X, Phinney AL, Manea M, *et al.* Therapeutically effective antibodies against amyloid-beta peptide target amyloid-beta residues 4-10 and inhibit cytotoxicity and fibrillogenesis. Nat Med 8: 1263-9 (2002).

[16] Morgan D, Diamond DM, Gottschall PE, Ugen KE, Dickey C, Hardy J, *et al.* A beta peptide vaccination prevents memory loss in an animal model of Alzheimer's disease. Nature 408: 982-5 (2000).

[17] Younkin SG. Amyloid beta vaccination: reduced plaques and improved cognition. Nat Med 7: 18-9 (2001).

[18] Holmes C, Boche D, Wilkinson D, Yadegarfar G, Hopkins V, Bayer A, *et al.* Long-term effects of Abeta42 immunisation in Alzheimer's disease: follow-up of a randomised, placebo-controlled phase I trial. Lancet 372: 216-23 (2008).

[19] Roberson ED, Scearce-Levie K, Palop JJ, Yan F, Cheng IH, Wu T, *et al.* Reducing endogenous tau ameliorates amyloid beta-induced deficits in an Alzheimer's disease mouse model. Science 316: 750-4 (2007).

[20] Reisberg B, Ferris SH, de Leon MJ, Crook T. The Global Deterioration Scale for assessment of primary degenerative dementia. Am J Psychiatry 139: 136-9 (1982).

[21] Samuel W, Masliah E, Hill LR, Butters N, Terry R. Hippocampal connectivity and Alzheimer's dementia: effects of synapse loss and tangle frequency in a two-component model. Neurology 44: 2081-8 (1994).

[22] Ingelsson M, Fukumoto H, Newell KL, Growdon JH, Hedley-Whyte ET, Frosch MP, *et al.* Early Abeta accumulation and progressive synaptic loss, gliosis, and tangle formation in AD brain. Neurology 62: 925-31 (2004).

[23] Gomez-Isla T, Hollister R, West H, Mui S, Growdon JH, Petersen RC, *et al.* Neuronal loss correlates with but exceeds neurofibrillary tangles in Alzheimer's disease. Ann Neurol 41:17-24 (1997).

[24] Goedert M, Spillantini MG. Tau mutations in frontotemporal dementia FTDP-17 and their relevance for Alzheimer's disease. Biochim Biophys Acta 1502: 110-21 (2000).

[25] Hutton M. Molecular genetics of chromosome 17 tauopathies. Ann N Y Acad Sci 920: 63-73 (2000).

[26] Spillantini MG, Van Swieten JC, Goedert M. Tau gene mutations in frontotemporal dementia and parkinsonism linked to chromosome 17 (FTDP-17). Neurogenetics 2:193-205 (2000).

[27] Santacruz K, Lewis J, Spires T, Paulson J, Kotilinek L, Ingelsson M, *et al.* Tau suppression in a neurodegenerative mouse model improves memory function. Science 309: 476-81 (2005).

[28] Spires-Jones LT, de Calignon A, Matsui T, Zehr C, Pitstick R, Wu HY, *et al. In vivo* imaging reveals dissociation between caspase activation and acute neuronal death in tangle-bearing neurons. J Neurosci 28: 862-7 (2008).

[29] Barghorn S, Mandelkow E. Toward a unified scheme for the aggregation of tau into Alzheimer paired helical filaments. Biochemistry 41: 14885-96 (2002).

[30] Maeda S, Sahara N, Saito Y, Murayama M, Yoshiike Y, Kim H, *et al.* Granular tau oligomers as intermediates of tau filaments. Biochemistry 46: 3856-61 (2007).

[31] Sahara N, Maeda S, Murayama M, Suzuki T, Dohmae N, Yen SH, *et al.* ssembly of two distinct dimers and higher-order oligomers from full-length tau. Eur J Neurosci 25: 3020-9 (2007).

Received: November 25, 2009 Revised: December 24, 2009 Accepted: December 26, 2009